X-Ray Fluorescence Computed Tomography to Visualize the 3-D Distribution of Nanoparticles for Biomedical Use

Nanoparticles (NPs) are recently attracting attention in nanomedicine for cancer imaging and radiation therapy. Although in these fields it is very important to image the NPs accumulated in tumors, a decisive imaging technique has not yet been established. We have therefore developed an X-ray fluorescence computed tomography technique based on a multiple-pinholes scheme (mp-XFCT), which visualizes the 3-D distribution of NPs based on the pinhole camera principle using fluorescent X-rays emitted from elements such as I, Gd and Au which constitute NPs. The efficacy of the technique was demonstrated by a reconstructed image obtained by an mp-XFCT prototype system constructed at AR-NE7A.

An imaging method that combines X-ray fluorescence analysis with a computed tomography reconstruction data-processing technique, called XFCT, is regarded as a promising candidate for NP imaging. A recent report demonstrated that XFCT accurately imaged the distribution of Au-NPs injected into a tumor-bearing mouse in a postmortem animal study [1]. However, the data-acquisition protocol of the conventional XFCT takes too long because the data are obtained by sequentially scanning a sample on a point-by-point basis [2-6], preventing 3-D reconstruction. To overcome the problem, a method based on a pinhole design with a 2-D detector and full-field volumetric incident beam was proposed [7, 8]. Recently, we proposed multi-pinhole XFCT (mp-XFCT) to enhance the signal-to-noise ratio of the projection and accelerate the acquisition process. This approach simultaneously acquires multiple projections through a multi-pinhole collimator with a 2-D detector and full-field volumetric incident beam [9, 10].

The mp-XFCT system is composed of a rotational stage for sample positioning, a multi-pinhole collimator (seven pinholes were used in the present study), and a 2-D detector with multiple elements [9, 10]. **Figure 1** shows a schematic representation of the mp-XFCT setup. A monochromatic parallel incident beam, which entirely covers the object, is propagated in a direction parallel to the surface of the multi-pinhole collimator and 2-D detector. The NPs in the object are excited by the incident beam and isotropically emit X-ray fluorescence on de-excitation. The emitted X-ray fluorescence passing through the pinholes is acquired by the detector. Thus, each view produces multiple projections. The data acquisition process is repeated while rotating the object. The 3-D distribution of NPs is estimated by solving a system of arithmetic equations representing the quantitative relationship between the estimated NPs concentration and the measured fluorescence count by using the maximum-likelihood expectation-maximization algorithm [8].

We constructed the mp-XFCT imaging system at AR-NE7A. A PILATUS 100K (pixel size: 172×172 μm^2) was used as a detector. We paid attention to the L-shell fluorescence of Au (L_α: 9.71 keV, L_β: 11.4 keV) because the quantum efficiency of the PILATUS 100K around 10 keV is approximately 90%. We selected an incident energy of 25 keV, which was the minimum energy set in the beamline, so that the incident energy was as close as possible to the L-edge energy of Au within the allowable range to produce more L-shell fluorescence photons. The flux was approximately

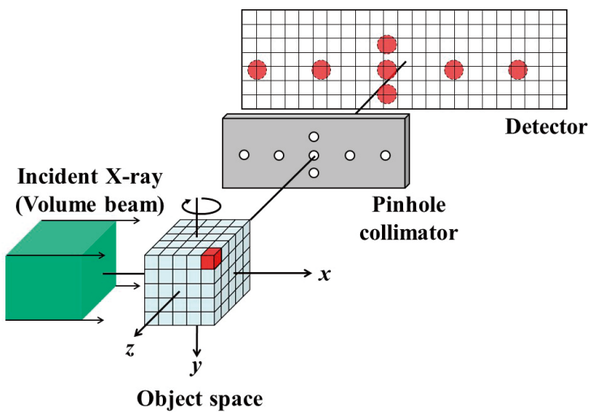

Figure 1: Schematic of mp-XFCT system.

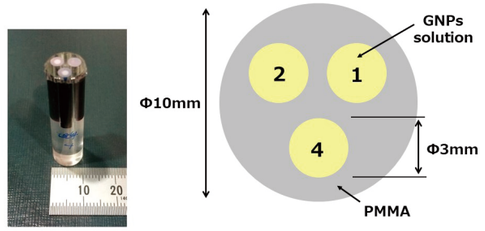

Figure 2: Physical phantom: photograph (left) and cross section (right).

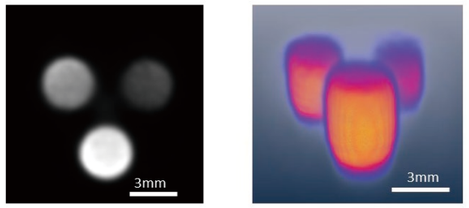

Figure 3: Reconstructed image: cross-sectional image (left), 3-D volume rendering image (right).

5.0×10^8 photons/mm^2/s in front of the object. The cross section of the incident beam was collimated to 35 mm (horizontal) × 5 mm (vertical) by the slit. The distance between the rotational axis and the collimator plane was 27.5 mm, and the distance between the collimator plane and the detector surface was 30.0 mm.

The physical phantom consisted of a 10-mm-diameter PMMA cylinder with three 3-mm-diameter channels filled with Au-NPs solution of different concentrations (1.0, 2.0, and 4.0 Au mg/ml), as shown in **Fig. 2**. Au-roVist™ (Nanoprobes, Inc., New York), for which the diameter of Au-NP was 15 nm, was used. The phantom was imaged with an exposure time per view of 1 min. One hundred and eighty projections were obtained at a constant angular step of 2° over 360°. The voxel size of the reconstructed image was 70×70×40 voxels; the edge of the voxel was 0.172 mm long, which was the same as the pixel dimension of the PILATUS detector [8, 9].

Figure 3 shows the cross sections at the central level of the 3-D reconstructed image and the 3-D image in the volume rendering (VR) representation. While the Au regions are distorted in the VR image, the distortion was mainly caused by the inhomogeneous distribution of intensity in the incident beam cross section. Analysis of the image revealed that the spatial resolution was about 0.3 mm. We obtained a satisfactory 3-D image.

In this study, we investigated the feasibility of *in vivo* imaging of gold nanoparticles for biomedical use. This preliminary study suggested that mp-XFCT could achieve a data-acquisition time of 20 min at a detection limit of approximately 0.1 Au mg/ml at a spatial resolution of 0.3 mm under an ideal experimental environment [10]. This finding is very encouraging for *in vivo* imaging of NPs. Next, we will focus on *ex vivo* imaging of biological organs containing Au-NPs.

REFERENCES

[1] N. Manohar, F. J. Reynoso, P. Diagaradjane, S. Krishnan and S. H. Cho, *Sci. Rep.* **6**, 22079 (2016).
[2] T. Yuasa, M. Akiba, T. Takeda, M. Kazama, A. Hoshino, Y. Watanabe, K. Hyodo, F. A. Dilmanian, T. Akatsuka and Y. Itai, *IEEE Trans. Nucl. Sci.* **44**, 54 (1997).
[3] Q. Huo, T. Yuasa, T. Akatsuka, T. Takeda, J. Wu, T.-T.-Lwin, K. Hyodo and F. A. Dilmanian, *Opt. Lett.* **33**, 2494 (2008).
[4] T. Takeda, J. Wu, T.-T.-Lwin, Q. Huo, T. Yuasa, K. Hyodo, F. A. Dilmanian and T. Akatsuka, *J. Synchrotron Rad.* **16**, 57 (2009).
[5] T.-T.-Lwin, T. Takeda, J. Wu, N. Sunaguchi, T. Murakami, S. Mouri, S. Nasukawa, Q. Huo, T. Yuasa, K. Hyodo and T. Akatsuka, *J. Synchrotron Rad.* **14**, 158 (2007).
[6] T.-T.-Lwin, T. Takeda, J. Wu, Q. Huo, T. Yuasa, K. Hyodo and T. Akatsuka, *J. Synchrotron Rad.* **15**, 528 (2008).
[7] N. Sunaguchi, T. Yuasa, K. Hyodo and T. Zeniya, *Opt. Comm.* **297**, 210 (2013).
[8] T. Sasaya, N. Sunaguchi, T.-T.-Lwin, K. Hyodo, T. Zeniya, T. Takeda and T. Yuasa, *Sci. Rep.* **7**, 44143 (2017).
[9] T. Sasaya, T. Sasaya, N. Sunaguchi, K. Hyodo, T. Zeniya and T. Yuasa, *Sci. Rep.* **7**, 5742 (2017).
[10] T. Sasaya, N. Sunaguchi, S.-J. Seoc, K. Hyodo, T. Zeniya, J.-K. Kim and T. Yuasa, *Nucl. Instrum. Methods Phys. Res. A* **886**, 71 (2018).

BEAMLINE

AR-NE7A

T. Sasaya[1], N. Sunaguchi[2], S. -J. Seo[3], T. Zeniya[4], K. Hyodo[5], J. -K. Kim[3] and T. Yuasa[1] ([1]Yamagata Univ., [2]Nagoya Univ., [3]Catholic Univ. of Daegu, [4]Hirosaki Univ. [5]KEK-IMSS-PF)